

Alpha particle emission in peripheral heavy ion reactions at 20 MeV/u

M. Bini

*Physics Department, University of Florence, Florence, Italy
and Lawrence Berkeley Laboratory, Berkeley, California 94720*

C. K. Gelbke and D. K. Scott

*Cyclotron Laboratory, Michigan State University, East Lansing, Michigan 48824
and Lawrence Berkeley Laboratory, Berkeley, California 94720*

T. J. M. Symons, P. Doll,* D. L. Hendrie, J. L. Laville,[†] J. Mahoney, M. C. Mermaz,[‡] C. Olmer,[§] K. Van Bibber,^{||} and H. H. Wieman

Lawrence Berkeley Laboratory, Berkeley, California 94720

(Received 12 May 1980)

The reaction $^{197}\text{Au}(^{16}\text{O},\text{HI}\alpha)$ has been investigated at 310 MeV. The angular correlations of alpha particles measured in coincidence with projectile-like fragments are very strongly forward peaked; the reaction is dominated by large negative values of the three-body Q value. Most of the observed alpha particles are emitted from projectile-like fragments. Within a factor of 2, no anisotropy of emission in the center-of-mass frame of the coincident projectile residue and alpha particle was found.

[NUCLEAR REACTIONS $^{197}\text{Au}(^{16}\text{O},\text{HI}\alpha)$, $E=310$ MeV; measured two-dimensional HI- α coincident energy and angular correlations; deduced reaction mechanisms.]

I. INTRODUCTION

From the numerous recent experimental and theoretical studies of light particle emission in heavy-ion collisions, it has become clear that these particles are an important source of information on the time evolution of the reaction mechanism from low energies close to the Coulomb barrier up to the highest available relativistic energies. Over the whole energy domain, there is an increasing emphasis on coincidence measurements, which refine the global insights derived from the earlier single particle inclusive experiments. In this paper we discuss such coincidence measurements between alpha particles and projectile-like fragments in reactions induced by ^{16}O on ^{197}Au at 310 MeV. This energy lies in the transitional region between low and high energy heavy-ion phenomena.¹ Some initial results of the experiments were reported earlier.²

At low energies, less than 5 MeV/u above the Coulomb barrier, the interaction time of the two colliding nuclei is longer than, or comparable to, the nuclear relaxation time of typically 10^{-21} sec.³⁻⁷ The dominant reaction mechanisms are established as deeply inelastic scattering or compound nucleus formation (see Refs. 3-7 and references therein). Here, the light particles are primarily emitted from the compound nucleus or from the fully accelerated and statistically equilibrated nuclei formed in deeply inelastic collisions.⁸⁻¹¹ Strictly speaking, these conclusions

are based on studies of heavy colliding nuclei ($A \geq 40$). For lighter nuclei, there is already evidence for a component of preequilibrium emission of light particles, even at energies below 5 MeV/u.^{12,13}

At higher energies, an increased, or even dominant, contribution is expected from preequilibrium processes, as established already in light-ion induced reactions.¹⁴⁻¹⁸ The decrease in the reaction time allows the excitation of higher lying states, which subsequently decay by particle emission rather than propagate into more complicated configurations. This possibility is less likely in low energy heavy-ion collisions, where the energy loss in each step is too small to lead to significant preequilibrium emission.¹⁹ There exists now a substantial body of data which demonstrate that nonequilibrium, light particle emission is an important aspect of heavy-ion collisions between 5 and 10 MeV/u, not only for deeply inelastic scattering²⁰⁻³² but also for incomplete fusion reactions.^{25, 33-39}

In spite of the wide variety of observed phenomena, a common feature in the experiments is the observation of angular correlations between alpha particles and projectile-like fragments that are not symmetric about the direction of the outgoing projectile residue. This asymmetry has been attributed to the emission of light particles from the contact zone between the two nuclei, prior to the subsequent deeply inelastic or fusion reaction. In a few cases,⁴⁰⁻⁴² evidence for this

emission by direct impact from the neck has also been found in collisions of heavy nuclei at energies much lower than 5 MeV/u.

The variety of phenomena has stimulated the development of many theoretical approaches, such as the "hot-spot" model,^{13, 22, 32, 43-46} the radial friction or "piston" model,⁴⁷ the promptly emitted particle (PEP) model,^{48, 49} and Fermi jets,^{50, 51} but detailed, quantitative comparisons with the data have been made for only a few cases.^{43, 48} These phenomenological models are probably more closely related than their derivations would suggest, and ultimately they must be derivable from more microscopically based preequilibrium and cascade theories, which are also successful in explaining some features of the data.^{21, 52} The relationship between preequilibrium and hot-spot models has already been discussed for light-ion reactions at intermediate energies.^{53, 54} In heavy-ion reactions there is also evidence for connecting links in experiments on inclusive proton emission in ¹⁶O induced reactions at 20 MeV/u,⁵⁵ which are successfully explained by preequilibrium emission as well as by emission from a hot source of nucleons moving independently of the target and projectile. The latter approach is closely related to the fireball concept invoked to explain light particle emission at relativistic energies,⁵⁶ and at the same time offers an alternative to the angle-dependent temperatures of the hot-spot models derived from the low energy data.^{22, 32, 53} The proton emission at 20 MeV/u has in fact also been explained by a stationary hot-spot model.⁵⁷

Close similarities of phenomena at 20 MeV/u (Refs. 1, 58, 59) and at relativistic energies⁶⁰ have also been demonstrated for the energy spectra of complex fragments which, at both energies, can be explained by a projectile breakup mechanism in which the target nucleus acts as a mere spectator.⁶¹⁻⁶⁵ At present, the relative importance of light particle production via breakup processes as compared to the more exotic mechanisms which were invoked in the explanation of the single particle inclusive data is not known. It is the object of this paper to provide more detailed experimental information through the measurement of alpha particle-projectile fragment coincidences for ¹⁶O induced reactions close to 20 MeV/u.

In this context, we will also establish a link to the potentially simpler case of light-ion induced reactions from the close similarities between the inclusive energy spectra for alpha particle⁶⁶⁻⁶⁸ or ⁶Li (Refs. 31, 69) induced reactions and for ¹⁶O induced reactions at 20 MeV/u. For light projectiles, the inclusive energy spectra are remarkably well described by the simple Serber model for

projectile breakup,^{66, 67} which is similar in spirit to the fragmentation models^{62, 64} applied to the case of heavy ions. However, subsequent investigations have shown that the elastic breakup channel is less important than inelastic or absorptive breakup.⁶⁸⁻⁷¹

In the present paper, we describe the results of coincidence experiments between alpha particles and projectile fragments in reactions induced by ¹⁶O on ¹⁹⁷Au at 310 MeV. The main features of our data are qualitatively similar to those observed for light ion induced reactions. The interaction of the fragments with the target nucleus will be shown to be an important aspect of the reaction mechanism. Similar to observations at lower energies,^{13, 20, 23, 24, 29} the angular correlations of coincident alpha particles observed in the laboratory are not symmetric about the direction of the outgoing projectile residue. Although such asymmetries may be taken as evidence for the preferential emission of alpha particles from the region of contact between the two colliding nuclei, we shall show that the asymmetries do not necessarily prove this point and that, indeed, we do not find convincing evidence for asymmetric emission of alpha particles in the rest frame of the outgoing projectile residue.

The next section of this paper gives the experimental details. In Sec. III, the overall qualitative trends of the data are presented. In Sec. IV, we discuss the effects of the primary fragment angular distributions and excitation energies on the angular correlations between projectile residues and alpha particles. A more detailed study of cross sections, transformed into the rest frame of the primary projectile-like fragments, is elaborated in Sec. V in order to reveal any evidence for isotropic or anisotropic emission from the primary fragment. The energy spectra observed in this rest frame are compared to a model calculation⁷² which gave the first theoretical interpretation for the experimentally observed similarities¹ between peripheral heavy ion reactions at 20 MeV/u and 2 GeV/u. Our results and conclusions are summarized in Sec. VI. Definitions of the various coordinate systems and kinematic transformations used in the paper are given in the Appendix.

II. EXPERIMENT

The experiment was performed at the 88-inch Cyclotron of the Lawrence Berkeley Laboratory. A ¹⁹⁷Au target of 15 mg/cm² thickness was bombarded by ¹⁶O⁶⁺ ions of 310 MeV energy. Outgoing projectile fragments were detected with a solid state telescope consisting of a ΔE detector of

51 μm thickness and an E detector of 3 mm thickness, which separated individual isotopes of elements from $Z=3$ to $Z=7$. This telescope subtended a solid angle of $\Omega=2$ msr and an angle of $\Delta\theta=2.9^\circ$ in the reaction plane. Coincident alpha particles were detected in two solid state detector telescopes consisting of 252 and 265 μm ΔE detectors and 5 mm E detectors. These telescopes subtended solid angles of $\Omega=1.2$ and 1.4 msr and angles of $\Delta\theta=2.4$ and 3.0 degrees, respectively, in the reaction plane. The events corresponding to alpha particle-projectile residue coincidences were stored on magnetic tape and analyzed off-line, and corrections were made to subtract random events and contributions from light target contaminants of carbon and oxygen. A cold trap at liquid nitrogen temperature was mounted close to the target in order to minimize the buildup of carbon and oxygen impurities. Even with this precaution, the contribution from carbon and oxygen contamination could not always be ignored, especially for very negative values of the three-body reaction Q value Q_3 in conjunction with correlation angles at which the alpha particle and the projectile residue were detected on opposite sides of the beam axis. In order to correct for these contaminants, the carbon and oxygen areal densities were determined to be 10 and 18 $\mu\text{g}/\text{cm}^2$ from a measurement of the Rutherford scattering of low energy alpha particles. The coincidence cross sections were also measured for a carbon target, and corrections were made assuming equal cross sections for the carbon and oxygen contaminants. An error of 25% is associated with these corrections. The magnitude of the correction was generally smaller than 30% approaching this value only for the most inelastic events considered in the analysis. Regions of Q values and correlation angles at which the magnitude of the contamination was larger than this value were not included in the analysis.

The absolute magnitude of the cross section is determined within 20%; the relative error bars plotted include statistical errors and errors due to the subtraction of random and contaminant events.

III. EXPERIMENTAL RESULTS

A. Energy spectra

Typical energy spectra of alpha particles detected in coincidence with carbon and boron projectile residues are shown in Figs. 1 and 2. The spectra are shown for the alpha particle detection angles of $\theta_\alpha = -10^\circ$, 9° , 25° , and 30° , and for the fixed detection angle $\theta_{\text{HI}} = 17^\circ$ for the coincident projectile residues. (Here, the convention is

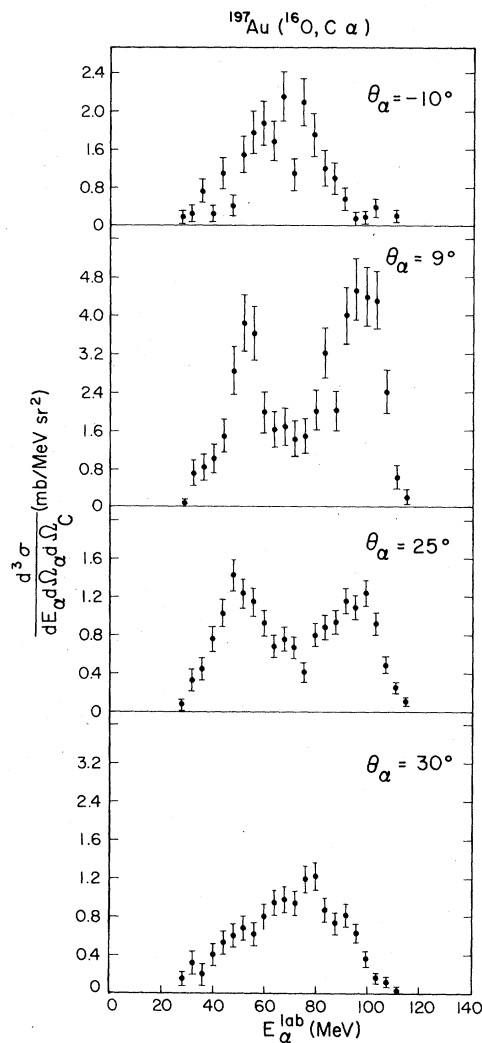


FIG. 1. Energy spectra of alpha particles measured for the reaction $^{197}\text{Au}(^{16}\text{O}, \text{C}\alpha)$ at 310 MeV. The carbon nuclei are detected at $\theta_c = 17^\circ$; the alpha particles are detected at $\theta_\alpha = -10^\circ$, 9° , 25° , and 30° .

adopted that positive values of θ_α correspond to alpha particles that are emitted on the same side of the beam axis as the projectile fragment; negative values of θ_α are used if the two coincident particles are detected on opposite sides with respect to the beam axis.)

The shapes of the alpha particle energy spectra depend very strongly on the detection angle. For alpha particles detected close to the outgoing projectile residue ($\theta_\alpha = 9^\circ$ and 25°) two peaks are observed in the energy spectra. Only one peak is observed for larger opening angles between the coincident nuclei; the position of this peak is intermediate between the locations of the two peaks that are observed for smaller correlation angles.

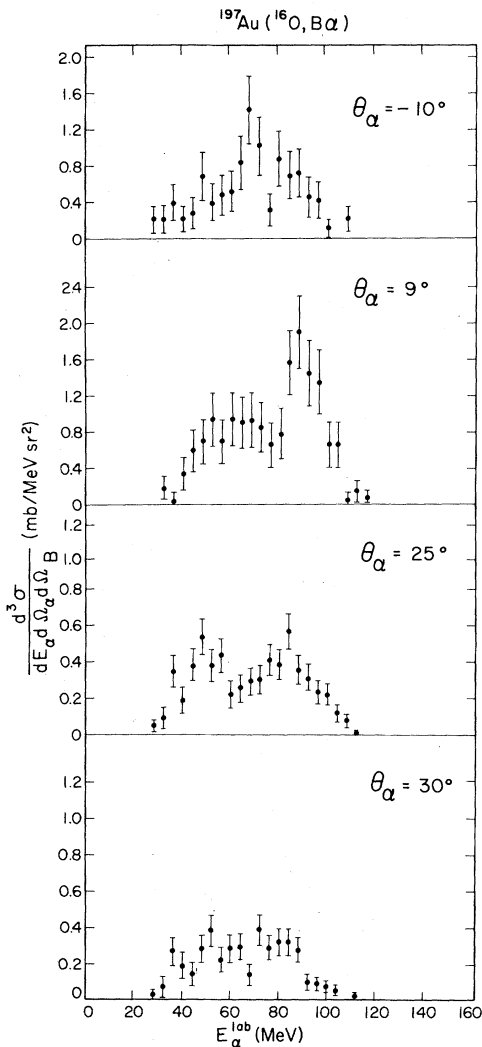


FIG. 2. Energy spectra of alpha particles measured for the reaction $^{197}\text{Au}(^{16}\text{O}, \text{B}\alpha)$ at 310 MeV. The boron nuclei are detected at $\theta_{\text{B}} = 17^\circ$; the alpha particles are detected at $\theta_{\alpha} = -10^\circ, 9^\circ, 25^\circ,$ and 30° .

These effects are particularly pronounced for C + α coincidences (Fig. 1) but are still present for B + α coincidences (Fig. 2).

This behavior is quite different from that of the $^{58}\text{Ni}(^{14}\text{N}, \text{H}\alpha)$ reaction at the lower energy of 148 MeV. For this reaction,²³ the coincidence cross section could be parametrized as the product of the singles cross sections for the detection of alpha particles and projectile residues. Such a parametrization implies that the energy spectra depend, for a given particle, only on the detection angle and not on the coincidence requirement, the physical interpretation being that the alpha particle is emitted from the contact zone at an early stage of the reaction, after which the heavy

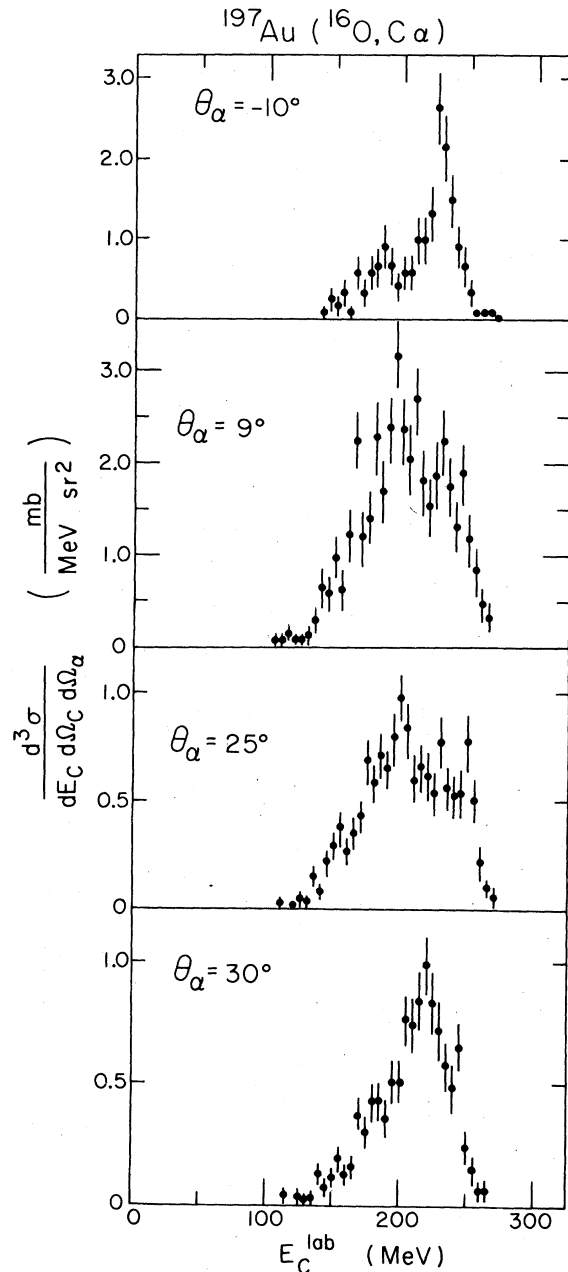


FIG. 3. Energy spectra of carbon nuclei measured for the reaction $^{197}\text{Au}(^{16}\text{O}, \text{C}\alpha)$ at 310 MeV. The carbon nuclei are detected at $\theta_{\text{C}} = 17^\circ$; the alpha particles are detected at $\theta_{\alpha} = -10^\circ, 9^\circ, 25^\circ,$ and 30° .

ions may undergo deeply inelastic scattering. The dramatic difference that is observed for the alpha particle energy spectra at -10° and 9° (i.e., $|\theta_{\alpha}| = 10^\circ$ and 9°) clearly rules out such a parametrization for the present data. In fact, the measured singles alpha particle spectra at all angles are of a monotonic, nearly exponential form.

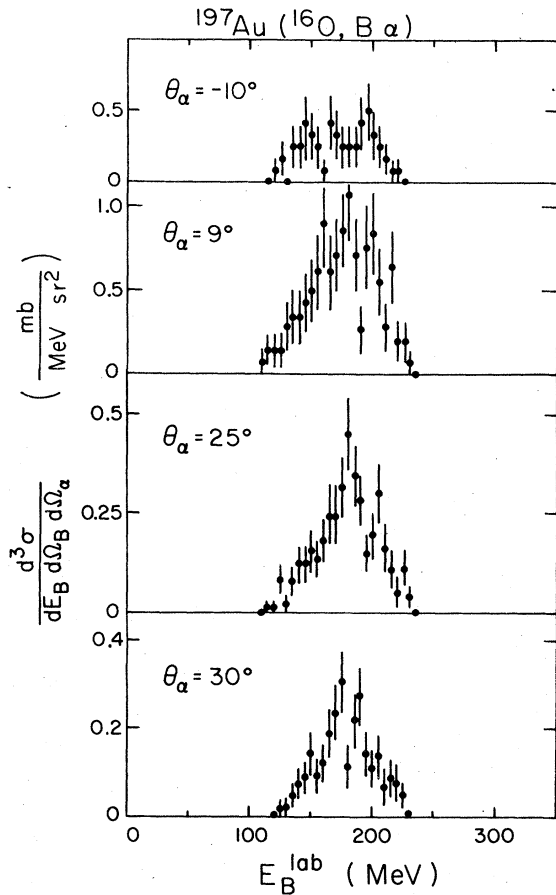


FIG. 4. Energy spectra of boron nuclei measured for the reaction $^{197}\text{Au}(^{16}\text{O}, \text{B}\alpha)$ at 310 MeV. The boron nuclei are detected at $\theta_{\text{B}} = 17^\circ$; the alpha particles are detected at $\theta_{\alpha} = -10^\circ, 9^\circ, 25^\circ, \text{ and } 30^\circ$.

Energy spectra of carbon and boron projectile residues detected in coincidence with alpha particles are shown in Figs. 3 and 4. These spectra were taken with the same coincidence conditions as those shown in Figs. 1 and 2 ($\theta_{\text{HI}} = 17^\circ$, $\theta_{\alpha} = -10^\circ, 9^\circ, 25^\circ, 30^\circ$). The detailed shapes of the carbon spectra also depend on the detection angle of the coincident alpha particle; the differences for the various coincidence conditions are, however, not so pronounced as for the alpha particle spectra. The shapes of the boron spectra are less dependent on the detection angle of the alpha particle.

B. Inelasticity of the reaction

The three-body reaction Q value Q_3 , as defined in Eq. (10) of the Appendix, can be used to specify the inelasticity of the reaction. It should be clear,

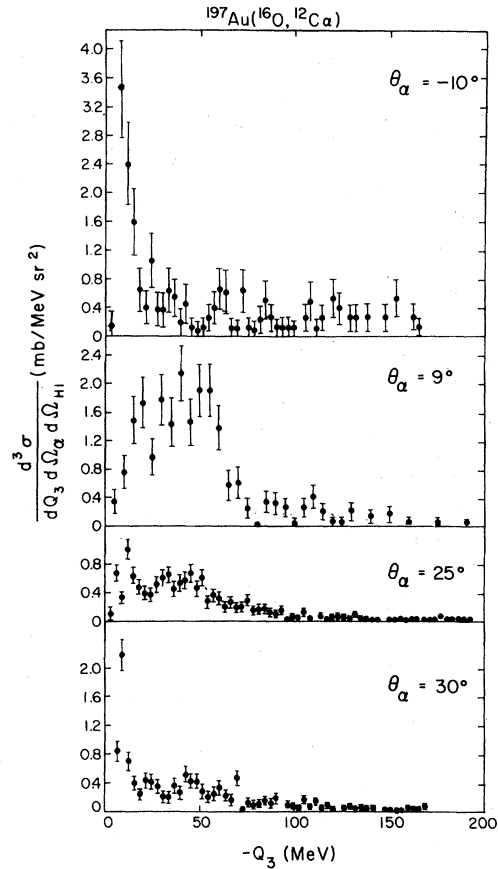


FIG. 5. Spectra of three-body reaction Q values Q_3 measured for the reaction $^{197}\text{Au}(^{16}\text{O}, ^{12}\text{C}\alpha)$ at 310 MeV. The outgoing ^{12}C nuclei were detected at the laboratory angle $\theta_{\text{C}} = 17^\circ$; the alpha particle detection angles θ_{α} are given in the figure.

however, that large negative values of Q_3 can arise both from large excitation energies of the target residue and from the production of more than three particles in the exit channel.

Spectra of Q_3 observed for various coincidence requirements are shown in Figs. 5–7. The shapes of these spectra depend on the mass and element numbers of the coincident projectile residue and on the detection angles of the two particles. The coincidence cross sections are mainly due to processes that involve relatively large negative values of Q_3 . (Although the $^{12}\text{C} + \alpha$ channel exhibits a strong quasielastic breakup component, it does not constitute the major part of the cross section.) “Elastic” breakup processes are, therefore, not the dominant mechanism. The fact that the interaction with the target is an important aspect of the reaction becomes particularly clear from a comparison of $^{12}\text{C} + \alpha$ and $^{13}\text{C} + \alpha$ cross sections, which

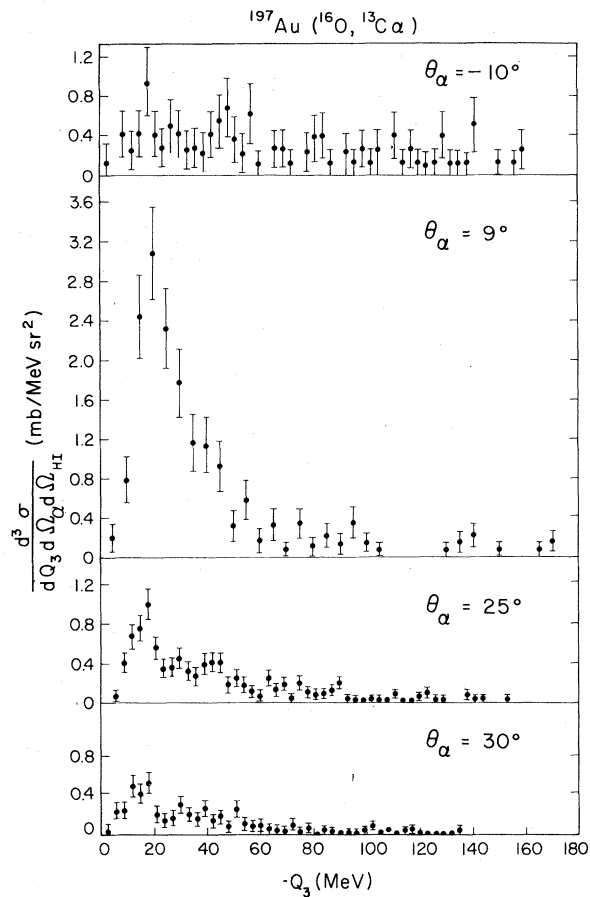


FIG. 6. Spectra of three-body reaction Q values Q_3 measured for the reaction $^{197}\text{Au}(^{16}\text{O}, ^{13}\text{C}\alpha)$ at 310 MeV. The outgoing ^{13}C nuclei were detected at the laboratory angle of $\theta_c = 17^\circ$; the alpha particle detection angles θ_α are given in the figure.

are very similar in magnitude. Whereas the $^{12}\text{C} + \alpha$ reaction could result from pure projectile fragmentation, the $^{13}\text{C} + \alpha$ channel must involve the transfer of at least one nucleon from the target.

In the Q_3 spectrum corresponding to the $^{12}\text{C} + \alpha$ reaction (Fig. 5), two components can be distinguished: a rather narrow quasielastic component ($Q_3 \geq -20$ MeV) and a more inelastic component ($Q_3 \leq -20$ MeV). Within the resolution and the statistics of the present experiment it is quite possible that the quasielastic component is dominated by, or even entirely due to, the elastic break-up process ($Q_3^{\text{elastic}} = -7.6$ MeV) that leads to the ground states of the three particles in the exit channel.

The two components observed for the $^{12}\text{C} + \alpha$ channel have distinctly different angular dependences, the elastic component being enhanced at the angles $\theta_\alpha = -10^\circ$ and $\theta_\alpha = +30^\circ$. For the other

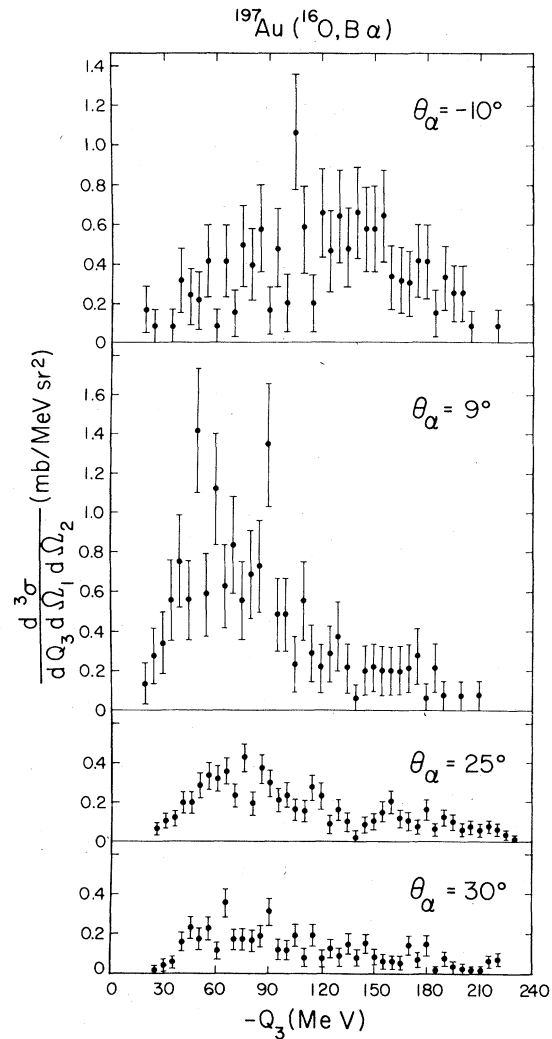


FIG. 7. Spectra of three-body reaction Q values Q_3 measured for the reaction $^{197}\text{Au}(^{16}\text{O}, \text{B}\alpha)$ at 310 MeV. The outgoing B nuclei were detected at the laboratory angle of $\theta_B = 17^\circ$; the alpha particle detection angles θ_α are given in the figure.

exit channels, a quasielastic component cannot be clearly identified.

C. Angular correlations

The energy integrated angular distributions of alpha particles that were detected in the reaction plane in coincidence with carbon, boron, and beryllium nuclei are shown in Fig. 8. These angular correlations are strongly peaked in the forward direction, but they are not symmetric about the beam direction or the direction of the detected heavy ion. They have a maximum at an angle that is intermediate between the direction

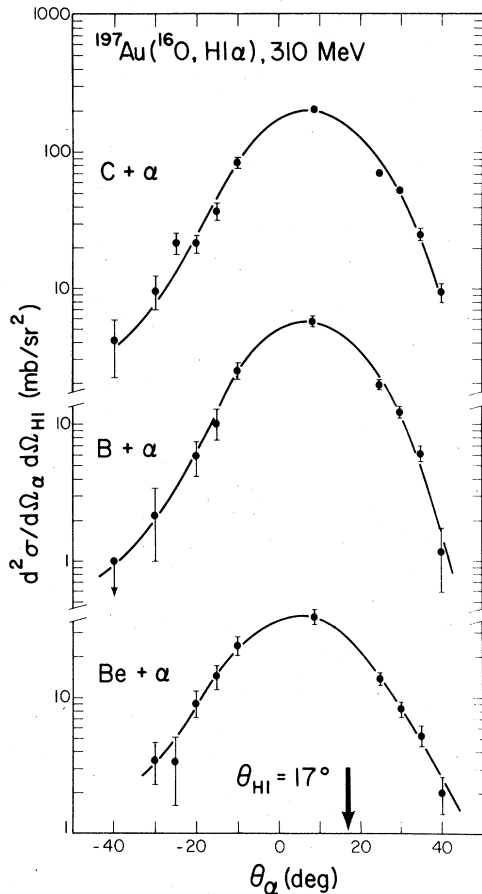


FIG. 8. Energy integrated in-plane angular correlations for the reaction $^{197}\text{Au}(^{16}\text{O}, \text{HI})\alpha$ at 310 MeV, HI = carbon, boron, and beryllium. The projectile residues HI are detected at $\theta_{\text{HI}} = 17^\circ$ (see arrow). Negative angles denote the detection of projectile residues and alpha particles on opposite sides with respect to the beam axis.

of the outgoing projectile residue ($\theta_{\text{HI}} = 17^\circ$, marked by an arrow in the figure) and the beam axis. In the present case, projectile fragments are expected to scatter to positive angles; therefore this correlation is contrary to the one expected from the "piston model" which predicts a maximum of the angular correlation if the two coincident particles emerge on opposite sides with respect to the beam axis and if only positive deflection angles occur.⁴⁷ The general shape of these angular distributions is similar to those observed in many of the reactions mentioned in the introduction.

The energy integrated angular correlations shown in Fig. 8 do not depend very strongly on the atomic numbers of the coincident projectile residue. More detailed information is obtained by

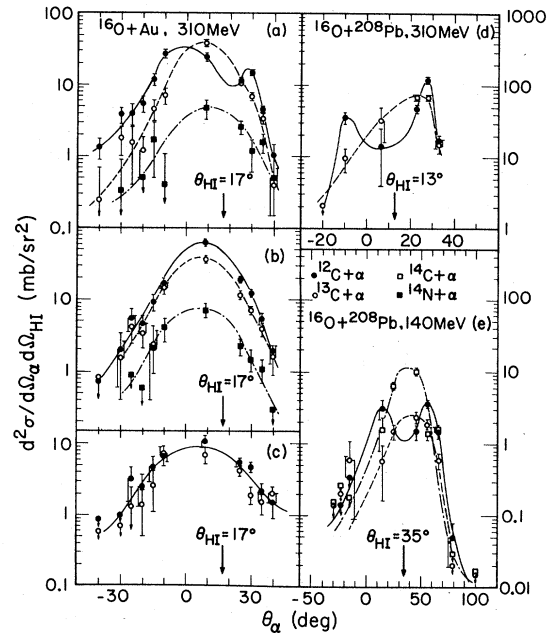


FIG. 9. In-plane angular correlations for ^{16}O induced reactions on ^{197}Au at 310 MeV [parts (a)–(c)] and on ^{208}Pb at 310 MeV [part (d)] and at 140 MeV [part (e)]. Three different regions of Q_3 values are displayed—group I [parts (a), (d), (e)]: $Q_3(\text{C} + \alpha) \geq -20$ MeV, $Q_3(\text{N} + \alpha) \geq -30$ MeV; group II [part (b)]: -60 MeV $\leq Q_3(\text{C} + \alpha) < -20$ MeV, -80 MeV $\leq Q_3(\text{N} + \alpha) < -30$ MeV; group III [part (c)]: -100 MeV $\leq Q_3(\text{C} + \alpha) < -60$ MeV.

plotting the angular correlations corresponding to different regions of the three-body Q value Q_3 and by separating the distributions associated with individual isotopes. In Fig. 9, the in-plane alpha particle angular correlations² are shown for ^{16}O induced reactions on ^{197}Au at 310 MeV [parts (a)–(c)] and on ^{208}Pb at 310 MeV [part (d)] and at 140 MeV [part (e)]. Three different regions of Q_3 values are displayed: group I [parts (a), (d), (e)], $Q_3(\text{C} + \alpha) \geq -20$ MeV, $Q_3(\text{N} + \alpha) \geq -30$ MeV; group II [part (b)], -60 MeV $\leq Q_3(\text{C} + \alpha) < -20$ MeV, -80 MeV $\leq Q_3(\text{N} + \alpha) < -30$ MeV; group III [part (c)], -100 MeV $\leq Q_3(\text{C} + \alpha) < -60$ MeV. There is a marked difference in shape between the angular correlation observed for the quasielastic $^{12}\text{C} + \alpha$ channel compared to all other channels. The quasielastic breakup channel $^{12}\text{C} + \alpha$ exhibits two maxima in the angular correlation for all three cases investigated [see full points in parts (a), (d), (e)]. For more negative Q_3 values, the $^{12}\text{C} + \alpha$ channels exhibit smooth, bell shaped angular correlations [see the full points in parts (b), (c)] similar to those observed for the other exit channels. The double peaked shape of the correlation for the quasielastic $^{12}\text{C} + \alpha$ channel is also observed for

⁶Li breakup reactions.

In order to observe this double peaked angular correlation, it is essential to study correlations for individual isotopes and to separate the quasi-elastic breakup component. From Fig. 9 it is clear that a superposition of distributions from different isotopes or from different regions of Q_3 values would wash out the double peaked signature of the quasielastic breakup process.

Although there is a marked difference in shape between the quasielastic $^{12}\text{C} + \alpha$ and $^{13}\text{C} + \alpha$ angular distributions, there is no significant difference in the magnitudes of the coincidence cross sections. Significantly smaller cross sections are, however, observed for the $^{14}\text{N} + \alpha$ channel.

IV. SCHEMATIC MODEL CONSIDERATIONS

Some of the features observed in the coincidence data can be explained by the simple picture of the quasifree breakup of the outgoing projectile-like fragment. Consider, for the sake of simplicity, the schematic picture of isotropic emission of monoenergetic light particles from a moving source, as sketched in Fig. 10. If the light particles are emitted close to the direction of the moving source, two peaks should be observed in the energy spectrum, resulting from forward and backward emission of the light particles in the rest frame of the moving source. With an increasing opening angle, the two energy peaks move closer together until they coincide at a limiting angle beyond which no particle can be detected. Close to this limiting angle the light particle angular distribution has a maximum due to the large volume of phase space for emission into this angular region. (It should be noted that other models also predict double peaked angular correlations. For example, in the hot-spot model,⁴³ two maxima are predicted in the angular correla-

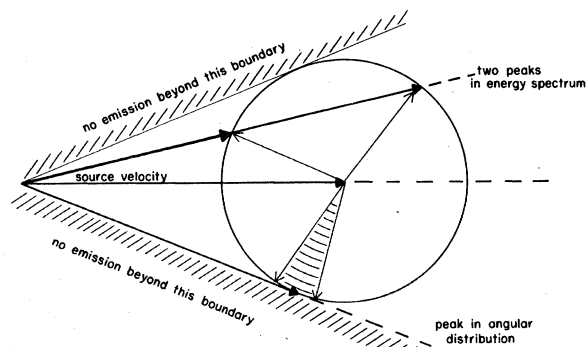


FIG. 10. The kinematic situation encountered for the ideal case of a moving source emitting monoenergetic light particles.

tions due to "shadowing" of the alpha particles emitted by the target and reabsorbed by the projectile, or vice versa. The effect discussed here does not involve such a complicated process but is rather of trivial kinematic origin.)

Some of the above features are clearly observed for the quasielastic $^{12}\text{C} + \alpha$ channel. The alpha particle energy spectra, measured at small relative angles between the outgoing alpha particle and ^{12}C nucleus, exhibit two peaks (see Fig. 1, $\theta_\alpha = 9^\circ$ and $\theta_\alpha = 25^\circ$), whereas only one peak is observed for larger opening angles (see Fig. 1, $\theta_\alpha = -10^\circ$ and $\theta_\alpha = 30^\circ$). At these larger opening angles, maxima are observed in the angular correlation as expected from the simple breakup model [see full points of Fig. 9(a)].

The alpha particle energy spectra observed in coincidence with projectile residues other than ^{12}C also exhibit similarities to the spectra of the $^{12}\text{C} + \alpha$ channel. Double peaked spectra are observed at $\theta_\alpha = 9^\circ$ but not at $\theta_\alpha = 30^\circ$. An example for the case of boron-alpha particle coincidences is shown in Fig. 2. However, the angular distributions are quite different since they have only one maximum; see Figs. 8 and 9. There are several possible reasons for these differences between the angular correlation for the quasielastic $^{12}\text{C} + \alpha$ breakup channel and the more complicated channels that are likely to involve large target excitations, nucleon transfer between target and projectile, or the emission of additional light particles: (i) Qualitatively different reaction mechanisms must be invoked for the quasielastic $^{12}\text{C} + \alpha$ channel and the other exit channels. (ii) The reaction mechanisms are qualitatively similar in all cases, but higher order processes and final state interactions are more important for those channels that differ from the quasielastic $^{12}\text{C} + \alpha$ breakup channel. (iii) The main differences observed for the various exit channels are due to different angular distributions and excitation energy spectra of freely decaying projectile residues. At present, there are no quantitative theories available that would allow us to distinguish between these options.

The alpha particle angular distributions observed at 310 MeV incident energy are not symmetric about the direction of the coincident projectile residue (see Figs. 8 and 9). This asymmetry does not necessarily imply that the emission of alpha particles in the center-of-mass frame of the heavy ion and the alpha particle is anisotropic. In particular, it cannot be concluded from this observation alone that the alpha particles emerge from the region of overlap between projectile and target although quantitative calculations for other cases suggest that such an emission

pattern may be favored by the experiments.^{20,29} However, the primary angular distribution of the prefragment can also have a drastic effect on the observed angular correlation.

The effect of the primary angular distribution on the observed angular correlation is illustrated schematically in Fig. 11. Here, we have calculated the decay of ^{16}O into $^{12}\text{C} + \alpha$ by assuming isotropic emission in the rest frame of the ^{16}O nucleus. For simplicity, the three-body reaction Q value was fixed at $Q_3 = -10$ MeV, and a kinetic energy release of $E_{12} = 4$ MeV was assumed. The angular distributions of the ^{16}O prefragments in the ($^{16}\text{O} + ^{197}\text{Au}$) center-of-mass frame were assumed in turn to be isotropic, Gaussian, or exponential. The parameters for the Gaussian and exponential shapes (shown on Fig. 11) are similar in magnitude to parameters that fit the observed inclusive angular distributions.¹ In Fig. 11, the calculated angular distributions of the primary fragments in the laboratory frame are shown by the dashed lines. The arrows denote the detection angle of the ^{12}C nucleus at $\theta_c = 17^\circ$, and the angular distribution of coincident alpha particles is shown by the solid lines. Quite clearly, strong asymmetries of the alpha particle angular cor-

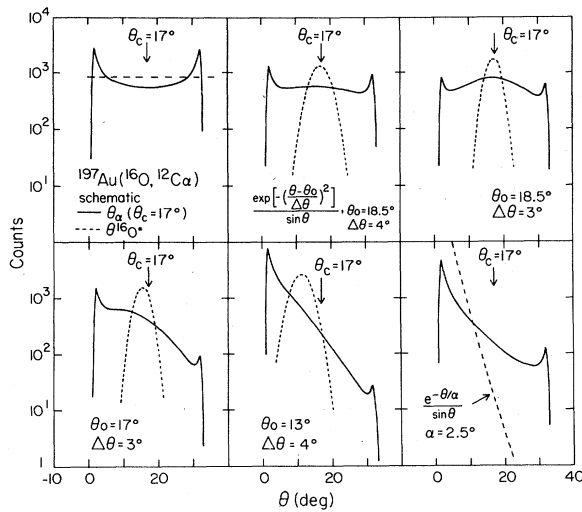


FIG. 11. The dependence of alpha particle angular correlations on the angular distribution of the primary ^{16}O nucleus, breaking up into $^{12}\text{C} + \alpha$, for the reaction $^{197}\text{Au}(^{16}\text{O}, ^{12}\text{C}\alpha)$ at 310 MeV. In the rest frame of the outgoing ^{16}O nucleus, isotropic emission in the reaction plane and a kinetic energy release of $E_{12} = 4$ MeV have been assumed. The three body reaction Q value was fixed to $Q_3 = -10$ MeV. The assumed primary ^{16}O angular distributions in the laboratory are indicated by dashed lines. The solid lines are the calculated alpha particle angular correlations if the coincident ^{12}C nucleus emerges at $\theta_c = 17^\circ$ (marked by arrows in the figure).

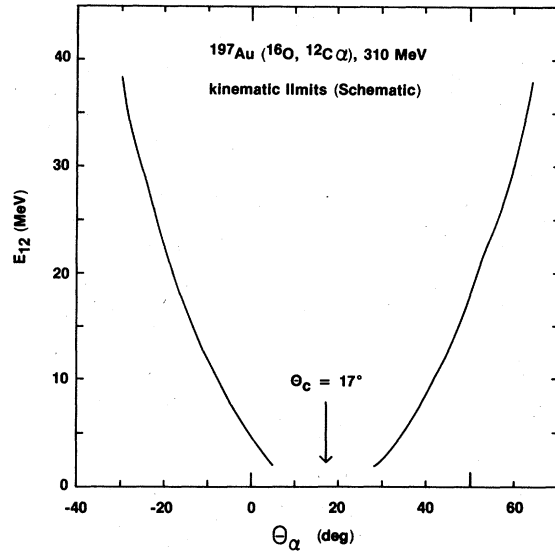


FIG. 12. The dependence of the positions of maxima in alpha particle angular correlations on E_{12} for the reaction $^{197}\text{Au}(^{16}\text{O}, ^{12}\text{C}\alpha)$ at 310 MeV. An isotropic angular distribution of the outgoing primary ^{16}O nuclei has been assumed—otherwise the assumptions are the same as in Fig. 12. The arrow marks the angle of the outgoing ^{12}C nucleus.

relations are produced if the ^{12}C nucleus is detected at an angle at which the angular distribution of the primary fragment has a steep slope. The alpha particle angular correlations are symmetric about the direction of the detected ^{12}C nucleus if the primary angular distribution is symmetric in the vicinity of the ^{12}C detection angle. In all cases, the angular correlations exhibit maxima close to the maximum opening angles between the two coincident particles, as expected from our earlier considerations of phase space.

The location of these maxima in the angular correlation depends on the spectrum of E_{12} , the relative kinetic energy between the two coincident fragments, and consequently on the excitation energy of the decaying nucleus, on the branching ratios and on the level densities of the decay products. The dependence of the location of the maximum of the angular correlation on E_{12} is illustrated in Fig. 12. From this strong dependence, it should be clear that the maxima in the angular correlations can be washed out if a broad range of relative kinetic energies contributes to the decay of the prefragment.

The effect of a continuous distribution of the relative kinetic energy on the shape of the angular correlation is illustrated in Fig. 13. The solid lines have been calculated with the distribution

$$P(E_{12}) = \begin{cases} 0, & \text{for } E_{12} \leq E_c \\ (E_{12} - E_c)^{1/2} e^{-(E_{12} - E_c)/T}, & \text{for } E_{12} > E_c \end{cases}$$

where $E_c = 2.5$ MeV and $T = 3$ MeV was assumed. From these model considerations it should be clear that the observed angular correlations can be strongly influenced by the distribution of relative kinetic energies. In particular, the maxima that are observed for the emission of monoenergetic light particles can almost completely disappear. For comparison we have included the predicted correlation for monoenergetic emission, $E_{12} = 4$ MeV, and also the angular distributions of the primary fragments for the cases of exponential and Gaussian shapes.

We do not attempt to fit our experimental angular correlations with this model since they could be influenced by many other effects. For example, the assumption of a unique Q_3 value is unrealistic. Furthermore, it is quite likely that interactions in the exit channel cannot be ignored. Ultimately, detailed models will be needed which incorporate all these effects. An extension of the theories⁷³ developed for the quantitative treatment of light-ion breakup to the case of heavy-ion reactions is definitely called for, and progress on this is already underway.⁶⁵ On the experimental side, it is clear that many of the features we have discussed for the energy spectra and angular distributions closely resemble the observations in breakup of ${}^6\text{Li}$ projectiles,³¹ including the double

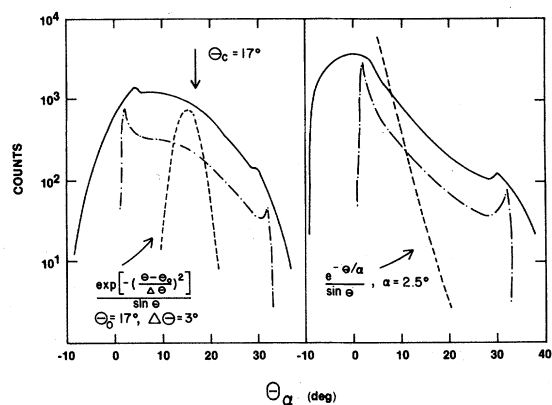


FIG. 13. The modification of alpha particle angular correlations by a continuous distribution of relative kinetic energies E_{12} . Dashed lines correspond to the assumed primary angular distribution; the dot-dash lines to the alpha particle angular correlation for constant value of $E_{12} = 4$ MeV; the solid lines to the alpha particle angular correlation for a continuous spectrum of energies E_{12} with spectral shape $P(E_{12}) = (E_{12} - E_c)^{1/2} \exp(-(E_{12} - E_c)/T)$ for $E_{12} > E_c = 2.5$ MeV, $T = 3$ MeV, and $P(E_{12}) = 0$ for $E_{12} < E_c$. Otherwise the assumptions are the same as in Fig. 12.

peaks in the energy spectra and angular distributions, as well as transfer reactions followed by breakup. Calculations for these processes must be performed before the observed coincidences between, for example, ${}^{14}\text{N}$ and alpha particles shown in Figs. 9(a) and 9(b) can be attributed to more exotic mechanisms like the "sparking" of alpha particles from the overlap zone of the colliding ions.

V. TRANSFORMATION OF CROSS SECTIONS INTO THE REST FRAME OF THE PRIMARY FRAGMENT

In the preceding section it was shown that some of the experimental observations were qualitatively consistent with isotropic light particle emission from the projectile-like fragment. It is justifiable, therefore, to transform the cross sections into the center-of-mass system of the alpha particle and heavy ion in order to highlight any deviations from isotropic emission.

A three dimensional polar plot of the angular dependence of the spectra for the relative kinetic energy E_{12} is shown in Fig. 14 for the case of ${}^{12}\text{C} + \alpha$ coincidences in which the carbon nucleus

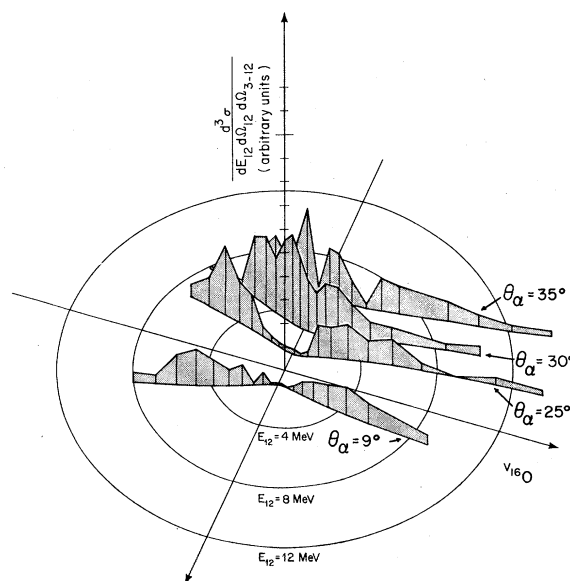


FIG. 14. The transformation of the ${}^{197}\text{Au}({}^{16}\text{O}, {}^{12}\text{C}\alpha)$ coincidence cross sections measured at 310 MeV incident energy into the ${}^{12}\text{C} + \alpha$ center-of-mass frame. The normalization between different ridges has been corrected for the estimated effects of the primary fragment angular distributions as described in the text. The cross sections are plotted in a polar diagram as a function of θ_{12} and E_{12} , as defined in the Appendix. The four ridges correspond to measurements at $\theta_\alpha = 9^\circ, 25^\circ, 30^\circ, 35^\circ$ with $\theta_c = 17^\circ$.

was detected at the fixed angle $\theta_c = 17^\circ$. The four ridges correspond to the alpha particle detection angles of $\theta_\alpha = 9^\circ, 25^\circ, 30^\circ,$ and 35° . Consequently, the angle between the $^{12}\text{C} + \alpha$ center-of-mass velocity and the beam axis has different values for different ridges; i.e., each ridge corresponds to a different average scattering angle of the primary fragment and, therefore, to a different cross section for the production of the primary fragment. This fact makes a direct comparison of the coincidence cross sections corresponding to different ridges very difficult. As a first attempt, the cross sections given in Fig. 14 were divided by the factor $e^{-\theta_f/\alpha}(\sin\theta_f)^{-1}$ to correct for the estimated angular distribution of the primary fragments, where θ_f is the c.m. scattering angle of the primary fragment and $\alpha = 5^\circ$ has been used. This is consistent with the slope of the ^{12}C inclusive angular distribution¹ (see discussion below). For fixed values of the detection angles θ_α and θ_c there is a slight dependence of θ_f on the kinetic energies of the two coincident particles; this variation was found to be relatively small (less than one degree). However, there is a large variation of θ_{12} with E_{12} ; i.e., the alpha particle emission angle in the $^{12}\text{C} + \alpha$ center-of-mass system varies considerably for a fixed detector setting. These facts make quantitative statements very difficult when only discrete sets of coincidence angle pairs are measured experimentally and when the heavy fragment detection angle is held fixed.

In order to proceed further, we note from Fig. 14 that the dependence of θ_{12} on E_{12} exhibits a rough forward-backward symmetry for a given detector geometry. Therefore, we compare the E_{12} spectra that correspond to emission into the forward and backward direction when viewed from the center-of-mass frame of the projectile residue and the alpha particle. These spectra are shown in Figs. 15–17 for $^{12}\text{C} + \alpha$, $^{13}\text{C} + \alpha$, and $\text{B} + \alpha$ coincidences and for the regions of Q values indicated (note that these spectra were not corrected for the estimated angular distributions of the primary fragments). The following notation has been adopted for labeling these spectra: B is the backward emission of the alpha particle; F, the forward emission of the alpha particle; L, the emission of the light particle to the left hand side with respect to the primary fragment velocity (i.e., the alpha particle emerges at a larger laboratory angle than the projectile residue); R, the emission of the light particle to the right hand side with respect to the primary fragment velocity (i.e., the alpha particle emerges at a smaller laboratory angle than the projectile residue or on the opposite side of the beam). The combina-

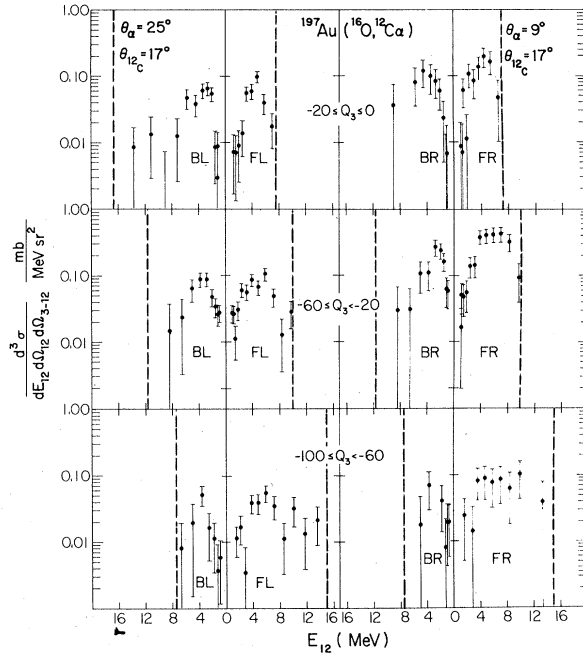


FIG. 15. Forward and backward emission cross sections for the reaction $^{197}\text{Au}(^{16}\text{O}, ^{12}\text{C}\alpha)$ at 310 MeV as viewed from the $^{12}\text{C} + \alpha$ center-of-mass frame. The quadrant labels BL, FL, BR, and FR are explained in the text and depicted in Fig. 21. The dashed lines indicate the detection limits due to detector thresholds.

tion of indices BL, for example, denotes emission into the backward left quadrant when viewed from the rest frame of the primary fragment (see also Fig. 21).

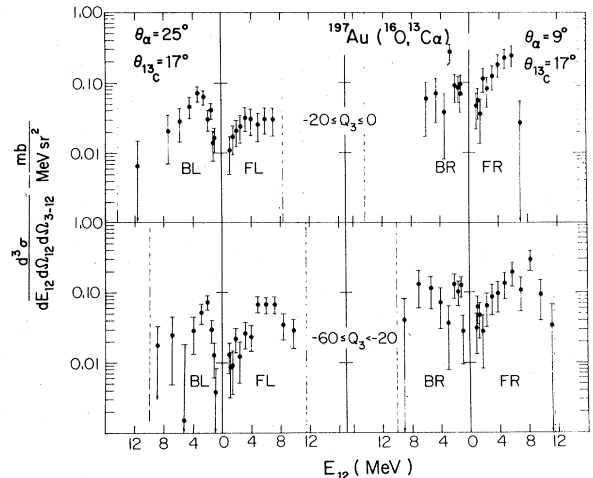


FIG. 16. Forward and backward emission cross sections for the reaction $^{197}\text{Au}(^{16}\text{O}, ^{13}\text{C}\alpha)$ at 310 MeV as viewed from the $^{13}\text{C} + \alpha$ center-of-mass frame. The quadrant labels BL, FL, BR, and FR are explained in the text and are depicted in Fig. 21. The dashed lines indicate the detection limits due to detector thresholds.

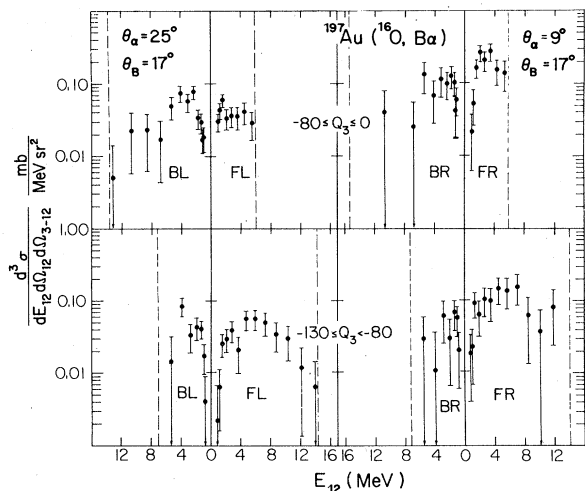


FIG. 17. Forward and backward emission cross sections for the reaction $^{197}\text{Au}(^{16}\text{O}, \text{B}\alpha)$ at 310 MeV as viewed from the $\text{B} + \alpha$ center-of-mass frame. The quadrant labels BL, FL, BR, and FR are explained in the text and depicted in Fig. 21. The dashed lines indicate the limits due to detector thresholds.

Two features are common to all the E_{12} spectra shown in Figs. 15–17: the cross sections exhibit a pronounced minimum for $E_{12} = 0$ and have maxima at E_{12} values of only a few MeV. The minimum at $E_{12} = 0$ could be due to the Coulomb repulsion between the coincident alpha particle and projectile residue. Alternatively, this minimum could result from the unavailability or weak population of states in the primary fragment which are close to the separation energy and decay into the corresponding particle channel. Additional experiments must be carried out with sufficient resolution to identify discrete states in the primary fragments in order to distinguish between these alternatives.

The low values of E_{12} suggest, however, that the two coincident particles are formed simultaneously and at a small distance from each other. This fact justifies, *a posteriori*, the discussion of the cross section in the center-of-mass frame of particles 1 and 2. We cannot, however, make the distinction between a direct breakup process and the sequential decay of the projectile-like fragment on the basis of the present observations alone.

The cross sections for emission into the forward and backward directions are of comparable magnitudes (see Figs. 15–17). It is by no means obvious that the small observed differences between the backward and forward emission spectra can be taken as a proof of anisotropic emission in the rest frame of the primary fragment. We have

already stressed that the comparison of these spectra is only approximate since the variation of θ_{12} with E_{12} is not exactly symmetric for forward and backward emission. Therefore, we conclude that there is symmetry between forward and backward emission within about a factor of 2. It is even more difficult to answer the question of a possible left-right asymmetry which would bear on the question of emission from a hot spot or from the contact zone of the projectile surface facing the target. The differences in cross sections that are already observed between the angle pairs $\theta_c = 17^\circ, \theta_\alpha = 25^\circ$ and $\theta_c = 17^\circ, \theta_\alpha = 9^\circ$ are mainly due to the different values of the c.m. emission angle θ_f of the primary fragment.

The strong dependence of the cross sections on the angle θ_f is illustrated in Fig. 18. The left hand side of the figure gives a comparison of the $^{12}\text{C} + \alpha$ cross sections measured for the detection angle pairs $\theta_c = 17^\circ, \theta_\alpha = 25^\circ$ and $\theta_c = 13^\circ, \theta_\alpha = 21^\circ$. In these two measurements the opening angle between the coincident particles has been left unchanged and both detectors have been shifted by 4° in the laboratory, causing a change of the primary fragment emission angles in the laboratory by 4° . This change in angle gives rise to a difference in the coincidence cross sections by one order of magnitude, which demonstrates the strong effect of the angular dependence of the

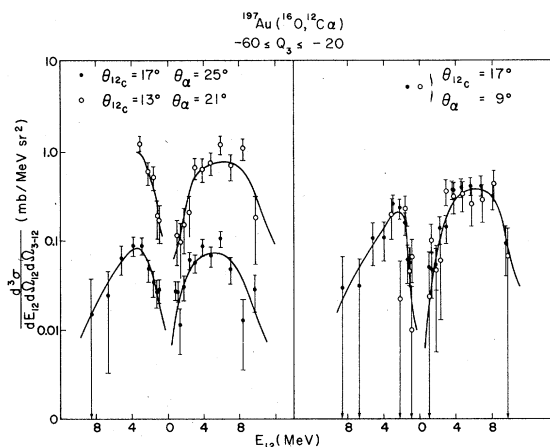


FIG. 18. Forward and backward emission cross sections for the reaction $^{197}\text{Au}(^{16}\text{O}, ^{12}\text{C}\alpha)$ at 310 MeV as viewed from the $\text{C} + \alpha$ center-of-mass frame. The effect of the primary fragment angular distribution is illustrated. The range of primary fragment emission angles θ_f is for the angle pair $\theta_\alpha = 25^\circ, \theta_c = 17^\circ$: $\theta_f = 19.7^\circ - 21.1^\circ$; for $\theta_\alpha = 21^\circ, \theta_c = 13^\circ$: $\theta_f = 15.9^\circ - 17.1^\circ$; for $\theta_\alpha = 9^\circ, \theta_c = 17^\circ$: $\theta_f = 15.7^\circ - 16.9^\circ$. (The finite opening angles of the detectors have not been taken into account.) Data corresponding to open and full points were taken with different detector thresholds accounting for the different energy cutoffs for backward emission.

primary fragment cross section. The right hand side of the figure gives the coincidence cross sections for the detection angle pair $\theta_c = 17^\circ$ and $\theta_\alpha = 9^\circ$ (two independent measurements with different detection thresholds are compared for consistency). From an event-by-event three-body kinematics analysis, the corresponding range of primary fragment angles in the laboratory is deduced as $15.7^\circ - 16.9^\circ$, ignoring the finite opening angles of the detectors. This should be compared with the measurement at $\theta_c = 13^\circ$ and $\theta_\alpha = 21^\circ$ in the left figure, which covers the very similar range of primary fragment emission angles, $15.9^\circ - 17.1^\circ$. These two measurements can, therefore, be used to assess the left-right asymmetry of the light particle emission. Again we have to stress that the comparison is not strictly quantitative since there remain differences between the other kinematic variables, and the range of θ_f is not weighted identically for the two measurements. However, we feel safe in concluding that, within a factor of 2, we do not find evidence for any left-right asymmetry for the light particle emission in the heavy ion-alpha particle center-of-mass frame.

We have attempted to correct the E_{12} spectra by assuming the angular distribution of the primary fragments to have the form

$$W(\theta_f) = \exp(-\theta_f/\alpha) / \sin\theta_f.$$

We used $\alpha = 5^\circ$ in order to make this parametrization consistent with the slope of the single particle inclusive angular distribution for outgoing carbon nuclei¹ and divided the observed cross sections by $W(\theta_f)$ to generate E_{12} spectra as described above. The resultant spectra for $^{12}\text{C} + \alpha$ coincidences are shown in Fig. 19. With these corrections we find very good agreement with the assumption of forward-backward and left-right symmetry of the light particle emission as viewed from the $^{12}\text{C} + \alpha$ center-of-mass system. In order to reveal the effects of asymmetries due to more exotic reaction mechanisms, the comparison with a theory must be made at a level of accuracy better than a factor of 2. In view of the difficulties mentioned above, it will be more appropriate to match the theoretical predictions to the experimental data in the laboratory frame.

As already mentioned in the Introduction, one can explain some of the similarities (and differences) observed for peripheral reactions of ^{16}O at 20 MeV/u and 2.1 GeV/u with a model that assumes the reaction to proceed in two stages.⁷² In the first stage, calculated within the framework of the Glauber model, a few surface nucleons in the overlap volume of projectile and target scatter and exchange energy and angular momentum. At

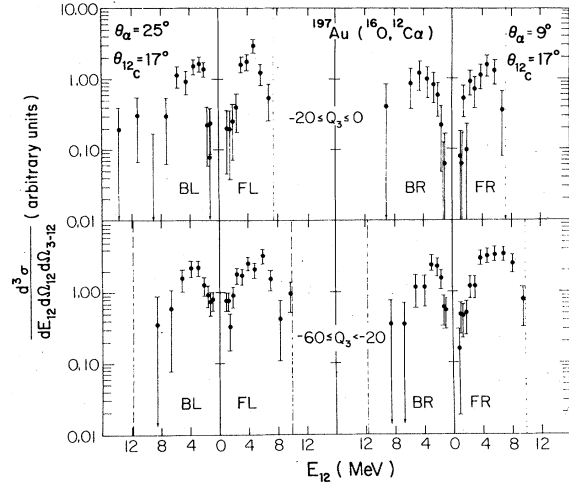


FIG. 19. Comparison of fore-aft and left-right emission asymmetries for the reaction $^{197}\text{Au}(^{16}\text{O}, ^{12}\text{C}\alpha)$ at 310 MeV as viewed from the $^{12}\text{C} + \alpha$ center-of-mass system. The estimated effects of the angular dependence of the primary cross sections have been corrected as described in the text. Detection limits are indicated by dashed lines. The quadrant labels BL, FL, BR, and FR are described in the text and depicted in Fig. 21.

the energy of 20 MeV/u, the knocked-on nucleons are not free to leave the prefragment but deposit all their energy and angular momentum into the prefragments which subsequently thermalize and decay statistically. The calculated⁷² excitation energy spectrum for $^{16}\text{O}^*$ prefragments can be converted into an E_{12} spectrum for $^{12}\text{C} + \alpha$ coincidences. The E_{12} spectra shown in Fig. 20 cor-

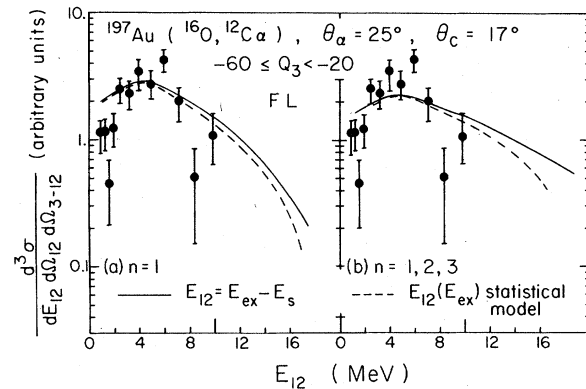


FIG. 20. E_{12} spectra for $^{12}\text{C} + \alpha$ coincidences predicted from Glauber model calculations (Ref. 72). Part (a) shows the distribution due to a single knock-on process; part (b) shows the result of including up to three knock-on processes in the calculation. The solid curves are calculated by assuming the decay to the ground state of ^{12}C only (when energetically allowed), and the dashed curves are the results from complete statistical model calculations.

respond to the excitation energy spectra of $^{16}\text{O}^*$ that are calculated including one or up to three knocked-on nucleons. The solid curves were obtained by assuming that all states above threshold decay to the ground state of ^{12}C ; the dashed curves are the result of a complete statistical model calculation. For comparison, we show the data of Fig. 19 which pertain to the situation FL, $-60 \text{ MeV} \leq Q_3 < -20 \text{ MeV}$. (The choice of this region of Q value seems most appropriate since both target and projectile should be excited according to the theory we are considering.) The experimental E_{12} distributions are seen to be in reasonable agreement with this simple model. Future investigations will have to show whether the model can also account for the observed angular correlations and Q_3 spectra.

VI. SUMMARY AND DISCUSSION

In this paper, we investigated the correlations between projectile residues and energetic alpha particles produced in ^{16}O induced reactions on heavy targets at 20 MeV/u incident energy. At the outset it was anticipated that correlation experiments at this incident energy might lead to enhanced contributions from reaction mechanisms such as the piston model, hot spot formation and decay, promptly emitted particles, or Fermi jets. However, within the limitations of the present experiment, our data do not show positive evidence for effects due to spatial localization or any other exotic reaction mechanism.

The shapes of the energy spectra were shown to depend strongly on the coincidence requirement and exhibited characteristics similar to those expected for isotropic emission from projectile-like fragments. The transformation of the cross sections into the center-of-mass system of the two coincident particles showed that the spectra of relative kinetic energies have pronounced minima at $E_{12} = 0$ and maxima at E_{12} values of only a few MeV. These results suggest that, for the majority of coincident particles detected in this experiment, the space-time separation at the point of emission is very small, which is consistent with the pictures of breakup reactions or decay of excited primary fragments.

The experimental angular correlations observed in the laboratory frame are not symmetric about the direction of the detected projectile residue. It was pointed out that such asymmetries could very well arise from the strong angular dependence of the primary fragment cross sections. The investigation of symmetric or asymmetric emission in the center-of-mass frame of the two coincident particles was found to be rather difficult due to the

interdependence of the various kinematic variables. Because of these difficulties a definite proof of symmetric emission is lacking. However, no large deviations from left-right and fore-aft symmetry of the light particle emission could be detected when the cross sections were transformed into the center-of-mass system of the coincident alpha particle and projectile residue and if the effects of the estimated primary heavy-ion angular distributions are taken into account. In particular, no evidence for more exotic effects like hot spots or shadowing could be established in our data.

The majority of alpha particles that are produced in coincidence with a projectile fragment do not originate from the elastic breakup process. The large negative values of Q_3 and the large cross sections for $^{13}\text{C} + \alpha$ coincidences, as well as significant $^{14}\text{N} + \alpha$ cross sections, show that the interaction with the target (inelastic scattering, nucleon transfer) is a dominant aspect of the reaction mechanism.

In the present experiment, only in-plane correlations were measured. Since these correlations are very sharply peaked in the forward direction and, furthermore, are asymmetric about both the beam axis and the direction of the coincident projectile residue, a complete set of out-of-plane measurements would be needed to provide reliable information about the alpha particle multiplicities. Such a measurement is beyond the scope of the present paper. However, rather large linear momentum transfer to the target residue has been observed⁷⁴ in peripheral reactions induced by ^{16}O on ^{238}U at 20 MeV/u. This large momentum transfer ($\approx \frac{2}{3}$ of the momentum lost by the projectile residue is transferred to the target) is not consistent with pure breakup reactions, in which all fragments are emitted as free particles in the exit channel. Instead, there must be a large probability for absorption by the target nucleus. These observations are reminiscent of the recent discovery^{31, 68-71} that light particle breakup reactions are dominated by "inelastic" and "absorptive" breakup processes. It should also be noted that energetic light particles are not only emitted in "peripheral" reactions in which the projectile residue is emitted into the exit channel but also in "central" collisions in which the major part of the projectile is captured by the target nucleus.^{24, 25, 34-37, 39} Rather similar energy spectra have been observed²⁵ for these two processes.

A uniform reaction mechanism might underlie all these phenomena—the breakup of the projectile, accompanied by a strong interaction with the target nucleus. This strong interaction could manifest itself by absorption of one of the frag-

ments, by inelastic excitation of the target residue or by nucleon transfer. An extension of the theories⁷³ developed for light particle breakup reactions to the case of heavy ions must be a first step towards an understanding of heavy ion reactions in the energy range above 10 MeV/u.

The experiments described in this paper were conducted at an incident energy in which previous inclusive measurements had already suggested the importance of projectile fragmentation. The coincidence experiments broadly confirm this picture. It is now clear, however, that absorptive and inelastic breakup processes are more important than the quasifree fragmentation model which adequately described the inclusive data. At lower incident energies, and for lighter systems, more exotic effects like emission from the contact zone, hot spots, shadowing, promptly emitted particles, and Fermi jets have been suggested as an explanation for energetic light particles. Our analysis shows that the problem of unraveling these exotic processes from much simpler mechanisms is nontrivial.

APPENDIX: COORDINATE SYSTEM AND TRANSFORMATIONS

In this section we define the three-body coordinate system and give explicit expressions for the relevant transformations that were used for the data reduction. (The notation and development of Ref. 75 will be followed.)

In the following equations, the subscripts 1, 2, and 3 denote the alpha particle, the outgoing projectile residue, and the recoiling target residue. Figure 21 shows the velocity vectors of these particles in the center-of-mass frame. If m_i , \vec{p}_i , and E_i denote the mass, momentum, and energy of particle i , we define the following reduced masses and momentum vectors:

$$M = m_1 + m_2 + m_3, \quad (1)$$

$$\mu_{ik} = m_i m_k / (m_i + m_k), \quad (2)$$

$$\mu_{l-ik} = m_l (m_i + m_k) / M, \quad (3)$$

$$\vec{P} = \vec{p}_1 + \vec{p}_2 + \vec{p}_3, \quad (4)$$

$$\vec{p}_{ik} = \mu_{ik} (\vec{p}_i / m_i - \vec{p}_k / m_k), \quad (5)$$

$$\begin{aligned} \vec{p}_{l-ik} &= \mu_{l-ik} [\vec{p}_l / m_l - (\vec{p}_i + \vec{p}_k) / (m_i + m_k)] \\ &= (m_i + m_k) \vec{P} / M - \vec{p}_i - \vec{p}_k \\ &= \vec{p}_l - m_l \vec{P} / M. \end{aligned} \quad (6)$$

Here, M is the total mass, \vec{P} is the total momentum \vec{p}_{l-ik} is the momentum vector of particle l with respect to the center-of-mass system of particles 1, 2, and 3, and \vec{p}_{ik} is parallel to the relative

velocity of particles i and k . (See Fig. 21 for illustration.)

The total kinetic energy is given by

$$\begin{aligned} E &= p_1^2 / 2m_1 + p_2^2 / 2m_2 + p_3^2 / 2m_3 \\ &= P^2 / 2M + E_{ik} + E_{l-ik}, \end{aligned} \quad (7)$$

where

$$E_{ik} = p_{ik}^2 / 2\mu_{ik} \quad (8)$$

is the relative kinetic energy of the particles i and k , and

$$E_{l-ik} = p_{l-ik}^2 / 2\mu_{l-ik} \quad (9)$$

is the kinetic energy of particle l in the center-of-mass system of all three particles, corrected for the recoil of particles i and k : $E_{l-ik} = E_l^{cm} M / (m_i + m_k)$. If we denote the projectile energy by E_p , we can define the three-body Q value Q_3 as

$$Q_3 = E - E_p. \quad (10)$$

At this point it is worth mentioning that all quantities can be defined in terms of the momenta and masses of the two particles 1 and 2 that are detected experimentally and in terms of the relations

$$\vec{p}_3 = \vec{P} - \vec{p}_1 - \vec{p}_2 = \vec{p}_p - \vec{p}_1 - \vec{p}_2 \quad (11)$$

and

$$m_3 = M - m_1 - m_2 = m_p + m_t - m_1 - m_2, \quad (12)$$

where the indices p and t denote projectile and target, respectively. If more than three particles are produced in the exit channel, \vec{p}_3 has to be interpreted as the total momentum of all unde-

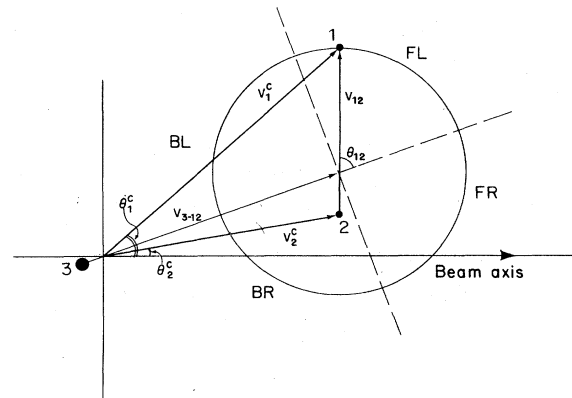


FIG. 21. Definition of velocity vectors for three-body kinematics. The velocities V_{12} and V_{3-12} are defined in terms of the momenta and generalized masses: $V_{12} = p_{12} / \mu_{12}$ and $V_{3-12} = p_{3-12} / \mu_{3-12}$. The index c denotes vectors in the center-of-mass system of the particles 1, 2, and 3.

tected particles and E_3 is the kinetic energy associated with the motion of the center-of-mass of these particles.

For a fixed value of Q_3 we can transform the triple differential cross sections as

$$\frac{d^3\sigma}{dE_{i_k}d\Omega_{i_k}d\Omega_{i-k}} = \frac{\mu_{i_k}p_{i_k}p_{i-k}}{m_i p_i p_k} \left[1 + \frac{\vec{p}_i \vec{p}_k}{p_k^2} - \frac{(m_i + m_k) \vec{P} \vec{p}_k}{M p_k^2} \right] \times \frac{d^3\sigma}{dE_i d\Omega_i d\Omega_k}, \quad (13)$$

and

$$\frac{d^3\sigma}{dE_{i_i}d\Omega_{i_i}d\Omega_{k-i}} = \frac{\mu_{i_i}p_{i_i}p_{k-i}}{m_i p_i p_k} \left(1 - \frac{m_k \vec{P} \vec{p}_k}{M p_k^2} \right) \times \frac{d^3\sigma}{dE_i d\Omega_i d\Omega_k} \quad (14)$$

In deriving Eqs. (13) and (14), we have used the

fact that the following Jacobians are unity:

$$\frac{\partial(\vec{P}, \vec{p}_{i-k}, \vec{p}_{i_k})}{\partial(\vec{p}_i, \vec{p}_k, \vec{p}_l)} = 1, \quad (15)$$

and

$$\frac{\partial(\vec{p}_{i-k}, \vec{p}_{i_k})}{\partial(\vec{p}_i, \vec{p}_k)} = 1. \quad (16)$$

ACKNOWLEDGMENTS

We would like to acknowledge the help of T. C. Awes in performing the model calculations shown in Figs. 11, 12, and 13. This material is based upon work supported by the National Science Foundation under Grant No. Phy 78-22696 and by the Office of Basic Energy Science and the Nuclear Physics Division of the U. S. Department of Energy. One of us (C. K. G.) acknowledges the receipt of an Alfred P. Sloan Fellowship.

*Present address: Institut für Kernphysik 1, Kernforschungszentrum, Karlsruhe, W. Germany.

†Permanent address: C.N.R.S., Caen, France.

‡Permanent address: C.E.N., Saclay, France.

§Present address: Department of Physics, Indiana University, Bloomington, Ind. 47401.

||Present address: Department of Physics, Stanford University, Stanford, Calif. 94305.

¹C. K. Gelbke, C. Olmer, M. Buenerd, D. L. Hendrie, J. Mahoney, M. C. Mermaz, and D. K. Scott, *Phys. Rep.* **42**, 311 (1978).

²C. K. Gelbke, M. Bini, C. Olmer, D. L. Hendrie, J. L. Laville, J. Mahoney, M. C. Mermaz, D. K. Scott, and H. H. Wieman, *Phys. Lett.* **71B**, 83 (1977).

³W. U. Schröder and J. R. Huizenga, *Annu. Rev. Nucl. Sci.* **27**, 465 (1977).

⁴V. V. Volkov, *Phys. Rep.* **44**, 93 (1978).

⁵W. U. Schröder, J. R. Birkelund, J. R. Huizenga, K. L. Wolf, and V. E. Viola, Jr., *Phys. Rep.* **45**, 301 (1978).

⁶M. Lefort and C. Ngô, *Riv. Nuovo Cimento* **2**, No. 12, 1 (1979).

⁷H. A. Weidenmüller, MPI-Report H-1978-V29, to be published in *Prog. Part. Nucl. Phys.*

⁸Y. Eyal, A. Gavron, I. Tserruya, Z. Fraenkel, Y. Eisen, S. Wald, R. Bass, G. R. Gould, G. Kreyling, R. Renfordt, K. Stelzer, R. Zitzmann, A. Gobbi, U. Lynen, H. Stelzer, I. Rode, and R. Bock, *Phys. Rev. Lett.* **41**, 625 (1978).

⁹D. Hilscher, J. R. Birkelund, A. D. Hoover, W. U. Schröder, W. W. Wilcke, J. R. Huizenga, A. C. Mignerey, K. L. Wolf, H. F. Breuer, and V. E. Viola, Jr., *Phys. Rev. C* **20**, 576 (1979).

¹⁰B. Tamain, R. Chechik, H. Fuchs, F. Hanappe, M. Morjean, C. Ngô, J. Péter, M. Dakowski, B. Lucas, C. Mazur, M. Ribrag, and C. Signarbieux, *Nucl. Phys.* **A330**, 253 (1979).

¹¹D. Guerreau, BNL Report No. BNL-5115, 1979, p. 59.

¹²J. W. Harris, T. M. Cormier, D. F. Geesaman, L. L. Lee, Jr., R. L. McGrath, and J. P. Wurm, *Phys. Rev.*

Lett. **38**, 1460 (1977).

¹³H. Ho, R. Albrecht, W. Dünnweber, G. Graw, S. G. Steadman, J. P. Wurm, D. Disdier, V. Rauch, and F. Scheibling, *Z. Phys.* **A283**, 235 (1977).

¹⁴G. D. Harp, J. M. Miller, and B. J. Berne, *Phys. Rev.* **165**, 1166 (1968).

¹⁵M. Blann and F. M. Lanzafame, *Nucl. Phys.* **A142**, 559 (1970).

¹⁶M. Blann, *Phys. Rev. Lett.* **27**, 337 (1971).

¹⁷C. K. Cline, *Nucl. Phys.* **A193**, 417 (1972).

¹⁸M. Blann, *Annu. Rev. Nucl. Sci.* **25**, 123 (1975).

¹⁹W. Nörenberg, *J. Phys.* **37**, C5-141 (1976).

²⁰A. Gamp, J. C. Jacmart, N. Poffé, H. Doubre, J. C. Roynette, and J. Wilczyński, *Phys. Lett.* **74B**, 215 (1978).

²¹J. B. Ball, C. B. Fulmer, M. L. Mallory, and R. L. Robinson, *Phys. Rev. Lett.* **40**, 1698 (1978).

²²T. Nomura, H. Utsunomiya, T. Motobayashi, T. Inamura, and M. Yanokura, *Phys. Rev. Lett.* **40**, 694 (1978).

²³R. K. Bhowmik, E. C. Pollacco, N. E. Sanderson, J. B. A. England, and G. C. Morrison, *Phys. Rev. Lett.* **43**, 619 (1979).

²⁴T. Inamura, T. Kojima, T. Nomura, T. Sugitate, and H. Utsunomiya, *Phys. Lett.* **84B**, 71 (1979).

²⁵T. C. Awes, C. K. Gelbke, B. B. Back, A. C. Mignerey, K. L. Wolf, P. Dyer, H. Breuer, and V. E. Viola, Jr., *Phys. Lett.* **87B**, 43 (1979).

²⁶B. Neuman, J. Buschmann, H. Klewe-Nebenius, H. Rebel, and H. J. Gils, *Nucl. Phys.* **A329**, 259 (1979).

²⁷R. Billerey, C. Cerruti, A. Chevarier, N. Chevarier, B. Cheynis, and A. Demeyer, *Z. Phys. A* **292**, 293 (1979).

²⁸A. Gamp, H. L. Harney, J. C. Roynette, E. Plagnol, H. Fuchs, H. Doubre, J. C. Jacmart, and N. Poffé, *Z. Phys. A* **291**, 347 (1979).

²⁹H. Ho, in *Proceedings of the Symposium on Deeply Inelastic and Fusion Reactions with Heavy Ions, Berlin*,

- 1979, edited by W. von Dertzen (Springer, Berlin, 1980).
- ³⁰G. A. Petit, R. L. Ferguson, A. Gavron, D. C. Hensley, F. E. Obenshain, F. Plasil, A. H. Snell, G. R. Young, K. A. Goeffroy, D. G. Sarantites, and C. F. Maguire, in *Proceedings of the Symposium on Continuum Spectra of Heavy Ion Reactions*, San Antonio, 1979 (unpublished).
- ³¹C. M. Castaneda, H. A. Smith, Jr., P. P. Singh, and H. Karwowski, *Phys. Rev. C* **21**, 179 (1980).
- ³²H. Utsunomiya, T. Nomura, T. Inamura, T. Sugitate, and T. Motobayashi, *Nucl. Phys.* **A334**, 127 (1980).
- ³³T. Inamura, M. Ishihara, T. Fukuda, T. Shimoda, and H. Hiruta, *Phys. Lett.* **68B**, 51 (1977).
- ³⁴D. R. Zolnowski, H. Yamada, S. E. Cala, A. C. Kahler, and T. T. Sugihara, *Phys. Rev. Lett.* **41**, 92 (1978).
- ³⁵H. Yamada, D. R. Zolnowski, S. E. Cala, A. C. Kahler, J. Pierce, and T. T. Sugihara, *Phys. Rev. Lett.* **43**, 605 (1979).
- ³⁶L. Westerberg, D. G. Sarantites, D. C. Hensley, R. A. Dayras, M. L. Halbert, and J. H. Barker, *Phys. Rev. C* **18**, 796 (1978).
- ³⁷D. G. Sarantites, L. Westerberg, M. L. Halbert, R. A. Dayras, D. C. Hensley, and J. H. Barker, *Phys. Rev. C* **18**, 774 (1978).
- ³⁸T. Nomura, J. Delaunay, C. Tosello, and N. Bendjaballah, *Nucl. Phys.* **A305**, 262 (1978).
- ³⁹K. Siwek-Wilczyńska, E. H. du Marchie von Voorthuyzen, J. van Popta, R. H. Siemssen, and J. Wilczyński, *Phys. Rev. Lett.* **42**, 1599 (1979).
- ⁴⁰J. M. Miller, G. L. Catchen, D. Logan, M. Rajagopalan, J. M. Alexander, M. Kaplan, and M. S. Zisman, *Phys. Rev. Lett.* **40**, 100 (1978).
- ⁴¹H. Delagrange, D. Logan, M. F. Rivet, M. Rajagopalan, J. M. Alexander, M. S. Zisman, M. Kaplan, and J. W. Ball, *Phys. Rev. Lett.* **43**, 1490 (1979).
- ⁴²M. Rajagopalan, L. Kowalski, D. Logan, M. Kaplan, J. M. Alexander, M. S. Zisman, and J. M. Miller, *Phys. Rev. C* **19**, 54 (1979).
- ⁴³P.-A. Gottschalk and M. Weström, *Phys. Rev. Lett.* **39**, 1250 (1977).
- ⁴⁴R. Weiner and M. Weström, *Nucl. Phys.* **A286**, 282 (1977).
- ⁴⁵P.-A. Gottschalk and M. Weström, *Nucl. Phys.* **A314**, 232 (1979).
- ⁴⁶W. U. Schröder, in *Proceedings of the Symposium on Continuum Spectra of Heavy Ion Reactions*, San Antonio, 1979 (unpublished).
- ⁴⁷D. H. E. Gross and J. Wilczyński, *Phys. Lett.* **67B**, 1 (1977).
- ⁴⁸J. P. Bondorf, J. N. De, A. O. T. Karvinen, G. Fai, and B. Jakobsson, *Phys. Lett.* **84B**, 162 (1979).
- ⁴⁹J. P. Bondorf, J. N. De, G. Fai, A. O. T. Karvinen, B. Jakobsson, and J. Randrup, *Nucl. Phys.* **A333**, 285 (1980).
- ⁵⁰W. J. Swiatecki, LBL Report No. LBL-8950, 1979.
- ⁵¹M. C. Robel, LBL Report No. LBL-8181, 1979.
- ⁵²H. W. Bertini, R. T. Santoro, and O. W. Hermann, *Phys. Rev. C* **14**, 590 (1976).
- ⁵³N. S. Wall, J. R. Wu, C. C. Chang, and H. D. Holmgren, *Phys. Rev. C* **20**, 1079 (1979).
- ⁵⁴N. Stelte, M. Weström, and R. M. Weiner, University of Marburg, report, 1979 (unpublished).
- ⁵⁵T. J. M. Symons, P. Doll, M. Bini, D. L. Hendrie, J. Mahoney, G. Mantzouranis, D. K. Scott, K. van Bibber, Y. P. Viyogi, H. H. Wieman, and C. K. Gelbke, *Phys. Lett.* **94B**, 131 (1980).
- ⁵⁶G. D. Westfall, J. Gosset, P. J. Johansen, A. M. Poskanzer, W. G. Meyer, H. H. Gutbrod, A. Sandoval, and R. Stock, *Phys. Rev. Lett.* **37**, 1202 (1976).
- ⁵⁷S. I. A. Garpman, D. Sperber, and M. Zielinska-Pfabe, *Phys. Lett.* **90B**, 53 (1980).
- ⁵⁸C. K. Gelbke, D. K. Scott, M. Bini, D. L. Hendrie, J. L. Laville, J. Mahoney, M. C. Mermaz, and C. Olmer, *Phys. Lett.* **70B**, 415 (1977).
- ⁵⁹D. K. Scott, M. Bini, P. Doll, C. K. Gelbke, D. L. Hendrie, J. L. Laville, J. Mahoney, A. Menchaca-Rocha, M. C. Mermaz, C. Olmer, T. J. M. Symons, Y. P. Viyogi, K. van Bibber, H. H. Wieman, and P. J. Siemens, LBL Report No. LBL-7729, 1978.
- ⁶⁰D. E. Greiner, P. J. Lindström, H. H. Heckman, B. Cork, and F. S. Bieser, *Phys. Rev. Lett.* **35**, 152 (1975).
- ⁶¹H. Feshbach and K. Huang, *Phys. Lett.* **47B**, 300 (1973).
- ⁶²A. S. Goldhaber, *Phys. Lett.* **53B**, 306 (1974).
- ⁶³D. F. Jackson, *Phys. Lett.* **71B**, 57 (1977).
- ⁶⁴K. W. McVoy and C. Nemes, *Z. Phys. A* **295**, 177 (1980).
- ⁶⁵T. Udagawa, T. Tamura, T. Shimoda, H. Fröhlich, M. Ishihara, and K. Nagatani, *Phys. Rev. C* **20**, 1949 (1979).
- ⁶⁶J. R. Wu, C. C. Chang, and H. D. Holmgren, *Phys. Rev. Lett.* **40**, 1013 (1978).
- ⁶⁷J. R. Wu, C. C. Chang, H. D. Holmgren, and R. W. Koontz, *Phys. Rev. C* **20**, 1284 (1979).
- ⁶⁸A. Budzanowski, G. Baur, C. Alderliesten, J. Bojowald, C. Mayer-Böricke, W. Oelert, P. Turek, F. Rösel, and D. Trautmann, *Phys. Rev. Lett.* **41**, 635 (1978).
- ⁶⁹B. Neumann, H. Rebel, J. Buschmann, H. J. Gils, H. Klewe-Nebenius, and S. Zagromski, *Z. Phys.* (to be published).
- ⁷⁰R. W. Koontz, C. C. Chang, H. D. Holmgren, and J. R. Wu, *Phys. Rev. Lett.* **43**, 1862 (1979).
- ⁷¹R. Shyam, G. Baur, F. Rösel and D. Trautmann, *Phys. Rev. C* **19**, 1246 (1979).
- ⁷²J. Hüfner, C. Sanders, and G. Wolschin, *Phys. Lett.* **73B**, 289 (1978).
- ⁷³G. Baur and D. Trautmann, *Phys. Rep.* **25**, 293 (1976).
- ⁷⁴P. Dyer, T. C. Awes, C. K. Gelbke, B. B. Back, A. Mignerey, K. L. Wolf, H. Breuer, V. E. Viola, Jr., and W. G. Meyer, *Phys. Rev. Lett.* **42**, 560 (1979).
- ⁷⁵G. G. Ohlsen, *Nucl. Instrum. Methods* **37**, 240 (1965).